

# Fluid Mechanics, Heat Transfer and Thermodynamic Issues of Micropipe Flows

A. Alper Ozalp

*Department of Mechanical Engineering, Uludag University,  
Turkey*

## 1. Introduction

Once the notion is aspired to examine the momentum and heat transfer characteristics of fluid flow in detail, the concept of energy mechanism is inevitably handled through both 1<sup>st</sup> and 2<sup>nd</sup> laws. Since the fundamental engineering phenomenon of internal flow is widely encountered in industrial installations, which may range from operations with non-Newtonian fluids (Yilbas & Pakdemirli, 2005) to heat exchangers (Stewart et al., 2005) and from geothermal district heating systems (Ozgener et al., 2007) even to micropipe systems (Kandlikar et al., 2003), the general scientific and technological frame of thermo-fluid operations has been in the consideration of several researchers. From methodological perspective, at macro level ( $d \geq 3$  mm), the explicit analytical correlations are capable of characterizing the flow and heat transfer issues of internal laminar flows. However, when the pipe diameter coincides with the micro range ( $d \leq 1$  mm) the order the pipe diameter and the level of surface roughness result in augmented entropy generation rates, besides give rise to substantial shifts in the velocity and temperature profiles from those of the characteristic recognitions, which as a consequence highlights the necessity in the identification of the so developed energy behaviors and the involved influential parameters related with the design, construction and operation of the object appliance.

Through experimental and computational investigations, involved researchers considered both the fluid flow and heat transfer mechanisms of micropipe flows. Kandlikar et al. (2003), for single-phase flow with small hydraulic diameters, studied the effects of surface roughness on pressure drop and heat transfer and concluded that transition to turbulent flows occurs at Reynolds number values much below 2300. Laminar and transitional flows in dimpled tubes were experimentally investigated by Vicente et al. (2002); the onset of transition at a relatively low Reynolds number of 1400 with 10% higher roughness induced friction factors when compared to the smooth tube ones were their primary findings. Engin et al. (2004) reported significant departures in the flow characteristics, from the conventional laminar flow theory, due to wall roughness effects in micropipe flows. The grow of friction coefficient with higher Reynolds number and lower hydraulic diameter were the theoretical and experimental evaluations of Renaud et al. (2008) in trapezoidal micro-channels. Guo & Li (2003) studied the mechanism of surface roughness provoked surface friction and concluded that the early transition from laminar to turbulent flow arose due to the frictional activity. Smooth micro-tubes under adiabatic conditions were experimentally investigated by Parlak et al. (2011); they determined that, as long as the viscous heating effects are taken

into account for micropipe diameters of  $d < 100 \mu\text{m}$ , the measured data and the calculated data from Hagen-Poiseuille equation of laminar flow are fairly comparable. The works of Celata et al. (2006a,b) described the roles of surface roughness on viscous dissipation, the resulting earlier transitional activity, augmented friction factor values and elevated head loss data. As the role of the cross-sectional geometry on viscous dissipation and the minimum Reynolds number for which viscous dissipation effects can not be neglected was considered by Morini (2005), Wu & Cheng (2003) reported the rise of laminar apparent friction coefficient and Nusselt number with the increase of surface roughness especially at higher Reynolds numbers. The significance of viscous dissipation on the temperature field and on the friction factor was studied numerically and experimentally by Koo & Kleinstreuer (2004). Obot (2002) reported that (i) onset of transition to turbulent flow in smooth microchannels does not occur if the Reynolds number is less than 1000, (ii) Nusselt number varies as the square root of the Reynolds number in laminar flow. Slit type microchannels were taken into experimental investigation by Almeida et al. (2010); their measurements for wide ranges of Reynolds number, hydraulic diameter and surface roughness proposed the systematic variation of frictional activity with micro structure and flow characteristics. Velocity slip and temperature jump phenomena in micro-flows were numerically investigated by Chen & Tian (2010). Wen et al. (2003) experimentally inspected the augmentation characteristics of heat transfer and pressure drop by the imposed wall heat flux, mass flux and different strip-type inserts in small tubes. Energy conversion of near-wall microfluidic transport for slip-flow conditions, including different channel aspect ratios, pressure coefficients and slip flow, were numerically considered by Ogedengbe et al. (2006). Petropoulos et al. (2010) carried out an experimental work on micropipe flows; in addition to reporting the variation of friction coefficient and pressure loss values with Reynolds number, they as well denoted the difficulties in sensitively measuring the velocity and pressure values. The influence of roughness level on the transition character in micropipe flows were recently reported by Celata et al. (2009); they as well added the appropriateness of Blasius and Colebrook equations for smooth and rough pipe cases respectively. In a more recent work Pitakarnnop et al. (2010) experimented micro-flows; they not only introduced a novel technique to enhance the measurement sensitivity but also compared their evaluations with different models for various gases and pressure ratios.

The thermodynamic issues of thermal systems are mostly interpreted through 2<sup>nd</sup> law analysis, where the concepts of frictional, thermal and total entropy generation rates are considered to be the particular parameters of the phenomena of exergy. Ko (2006a) carried out a numerical work on the thermal design of a double-sine duct plate heat exchanger, from the point of entropy generation and exergy utilization. Second law characteristics in smooth micropipe were experimentally investigated by Parlak et al. (2011); they recorded augmentations in entropy generation with higher Reynolds number and with lower micropipe diameter. Sahin (1998), for a fully developed laminar viscous flow in a duct subjected to constant wall temperature, inspected the entropy generation analytically. He reported the promoted entropy generation due to viscous friction and further determined that the dependence of viscosity on temperature becomes essentially important in accurately evaluating the entropy generation. Richardson et al. (2000), in singly connected microchannels with finite temperature differences, investigated the existence of an optimum laminar frictional flow regime, based on 2<sup>nd</sup> law analysis. In computing the process irreversibility or loss of exergy, Kotas et al. (1995) validated the applicability of exergy balance, or the Gouy-Stodola theorem. Ratts & Raut (2004) employed the entropy generation

minimization method and obtained optimal Reynolds numbers for single-phase, fully developed internal laminar and turbulent flows with uniform heat flux. The association of structural, thermal and hydraulic issues with entropy generation was described by Avci & Aydin (2007), who performed 2<sup>nd</sup> law calculations in hydrodynamically and thermally fully developed micropipe flows. In a similar study, Hooman (2008) as well computationally inspected the local and overall entropy generation in a micro-duct and reported the variation of entropy generation and Bejan number with Reynolds number, wall heat flux and hydraulic diameter. Tubular heat exchanger with enhanced heat transfer surfaces were investigated by Zimparov (2000), who aimed to enlighten the effects of streamwise variation of fluid temperature and rib height to diameter ratio on the entropy production. Sahin et al. (2000) studied entropy generation due to fouling as compared to that for clean surface tubes. To determine the optimal Reynolds number with least irreversibility and best exergy utilization, Ko (2006b) numerically investigated the laminar forced convection and entropy generation in a helical coil with constant wall heat flux.

Although the significance and the concurrent impact of pipe diameter ( $d$ ) and surface roughness ( $\epsilon$ ) in micropipe flows is known for a long time, the basics and the individual and combined roles of  $d$  and  $\epsilon$  on the fluid motion and heat transfer mechanisms of fluid flow in circular micro-ducts are not revealed yet. This computational study is a comprehensive investigation focusing on the roughness induced forced convective laminar-transitional micropipe flows. The work is supported by the Uludag University Research Fund and aims not only to investigate and discuss the fluid mechanics, heat transfer and thermodynamic issues but also to develop a complete overview on the 1<sup>st</sup> and 2<sup>nd</sup> law characteristics of flows in micropipes. Analysis are performed for the micropipe diameter, non-dimensional surface roughness ( $\epsilon^* = \epsilon/d$ ), heat flux ( $q''$ ) and Reynolds number ( $Re$ ) ranges of  $0.50 \leq d \leq 1.00$  mm,  $0.001 \leq \epsilon^* \leq 0.01$ ,  $1000 \leq q'' \leq 2000$  W/m<sup>2</sup> and  $100 \leq Re \leq 2000$  respectively. As the evaluations on fluid motion are interpreted through radial distributions of axial velocity, boundary layer parameters and friction coefficients, heat transfer results are displayed with radial temperature profiles and Nusselt numbers. Thermodynamic concerns are structured through 2<sup>nd</sup> law characteristics, where cross-debates on thermal, frictional and total entropy generation values and Bejan number are carried out by enlightening the features of structural ( $d$  &  $\epsilon^*$ ), fluid motion ( $Re$ ) and energetic ( $q''$ ) agents. The scientific links among the fluid mechanics parameters, the heat transfer characteristics and the thermodynamic concepts are as well discussed in detail to develop a complete overview of micropipe flows for various micropipe diameter, surface roughness, heat flux and Reynolds number cases.

## 2. Theoretical background

### 2.1 The geometry: micropipe and roughness

The numerical analyses are performed for the micropipe geometry with the length and diameter denoted by  $L$  and  $d$  respectively (Fig. 1(a)). The roughness (Fig. 1(b)) is characterized by the two denoting parameters of roughness amplitude ( $\epsilon$ ) and period ( $\omega$ ). The outline model is equilateral-triangular in nature (Cao et al., 2006), such that the roughness periodicity parameter ( $\omega' = \omega/\epsilon$ ) is kept fixed to  $\omega' = 2.31$  throughout the study. The implementation of the amplitude and period are defined by Eq. (1), which defines the model function  $f_\epsilon(z)$ . The Kronecker unit tensor ( $\delta_i$ ) attains the values of  $\delta_i = +1$  and  $-1$  for  $0 \leq z \leq \frac{2.31}{2}\epsilon$

and  $\frac{2.31}{2}\epsilon \leq z \leq 2.31\epsilon$  respectively, utilizing the streamwise repetition of  $f_\epsilon(z)$  throughout the pipe.

$$f_\epsilon(z) = \delta_i \epsilon \left[ 1 - \frac{4}{2.31\epsilon} z \right] \tag{1}$$

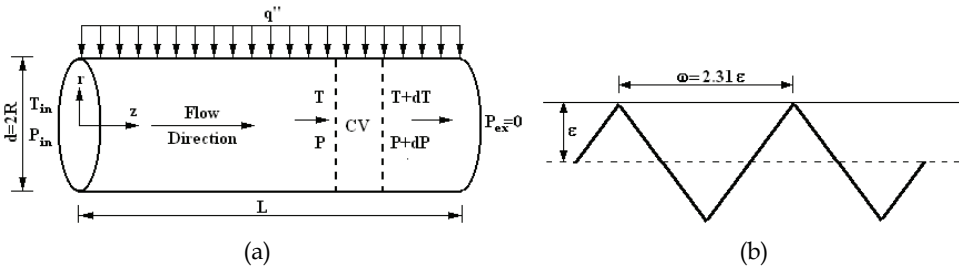


Fig. 1. (a) Schematic view of micropipe, (b) triangular surface roughness distribution

**2.2 Fundamental formulations**

The problem considered here is steady ( $\partial/\partial t = 0$ ), fully developed and the flow direction is coaxial with pipe centerline ( $U_r = U_\theta = 0$ ), thus the velocity vector simplifies to  $\vec{V} = U_z(r)\hat{k}$ , denoting that the flow velocity does not vary in the angular ( $\partial U_z/\partial \theta = 0$ ) and axial ( $\partial U_z/\partial z = 0$ ) directions. These justifications are common in several recent numerical studies, on roughness induced flow and heat transfer investigations, like those of Engin et al. (2004), Koo & Kleinstreuer (2004) and Cao et al. (2006). The working fluid is water; thus the incompressible formulations, with the constant density approach ( $\rho = \text{constant}$ ), are employed throughout the study. In the present incompressible flow application with constant pipe diameter, the viscous stress ( $\tau_{zz}$ ) vanishes due to the unvarying local and cross-sectional average velocities ( $\partial U_z/\partial z = 0$ ) in the flow direction; thus for fully developed laminar incompressible flow the continuity, momentum and energy equations are given by the Eqs. (2), (3) and (4) respectively.

$$\frac{\partial}{\partial z}(U_z) = 0 \tag{2}$$

$$\frac{\partial P}{\partial z} = \frac{1}{r} \frac{\partial}{\partial r}(r\tau_{rz}) \tag{3}$$

$$\rho U_z \frac{\partial}{\partial z} \left( e + \frac{P}{\rho} + k \right) + \frac{1}{r} \frac{\partial}{\partial r}(r q_r'') + \frac{\partial q_z''}{\partial z} = \tau_{rz} \frac{\partial U_z}{\partial r} + U_z \left[ \frac{1}{r} \frac{\partial}{\partial r}(r\tau_{rz}) \right] \tag{4}$$

In Eqs. (2-3), as the viscous stress tensor ( $\tau_{rz}$ ) and heat flux terms ( $q_r''$ ,  $q_z''$ ) are given by Eqs. (5a-c), the internal and kinetic energy terms are defined as  $e = C_p T$  and  $k = U_z^2/2$ , respectively.

$$\tau_{rz} = \mu^T \frac{\partial U_z}{\partial r} \quad q_r'' = -\kappa_f^T \frac{\partial T}{\partial r} \quad q_z'' = -\kappa_f^T \frac{\partial T}{\partial z} \quad (5a-c)$$

As given in Fig. 1(a), at the pipe inlet, pressure ( $P_{in}$ ) and temperature ( $T_{in}$ ) values are known and the exit pressure ( $P_{ex}$ ) is atmospheric. The flow boundary conditions are based on the facts that, on the pipe wall ( $r=R$ ) no-slip condition and constant heat flux ( $q''$ ) exist, and flow and thermal values are maximum at the centerline ( $r=0$ ). Denoting  $U_z=U_z(r)$  and  $T=T(r,z)$ , the boundary conditions can be summarized as follows:

$$r = R + f_e(z) \rightarrow U_z = 0 \quad \& \quad r = 0 \rightarrow \frac{\partial U_z}{\partial r} = 0 \quad (6a)$$

$$r = R + f_e(z) \rightarrow \frac{\partial T}{\partial r} = -\frac{q_r''}{\kappa_f^T} \quad \& \quad r = 0 \rightarrow \frac{\partial T}{\partial r} = 0 \quad (6b)$$

$$z = 0 \rightarrow P = P_{in}, T = T_{in} \quad \& \quad z = L \rightarrow P_{ex} = 0 \text{ (Man.)} \quad (6c)$$

The average fluid velocity ( $U_o$ ) and temperature ( $T_o$ ), at any cross-section in the pipe, are defined as

$$U_o = \frac{2\pi \int_{r=0}^{r=R} U_z(r)rdr}{\pi R^2} \quad T_o = \frac{2\pi \int_{r=0}^{r=R} U_z(r)C_p(r)T(r)rdr}{U_o(C_p)_o \pi R^2} \quad (7a-b)$$

and the shear stress ( $\tau$ ) and mass flow rate ( $\dot{m}$ ) are obtained from

$$\tau = C_f \frac{1}{2} \rho U_o^2 = \mu^T \left| \frac{dU_z}{dr} \right|_{r=R} \quad \dot{m} = \rho U_o A = \rho 2\pi \int_{r=0}^{r=R} U_z(r)rdr \quad (8a-b)$$

where  $C_f$ ,  $\rho$  and  $A$  stand for friction coefficient, density and cross-sectional area respectively.

Denoting the surface and mean flow temperatures as  $T_s$  and  $T_o$ , identifying the thermal conductivity and convective heat transfer coefficient with  $\kappa_f$  and  $h$ , and labeling dynamic and kinematic viscosity of water by  $\mu$  and  $\nu$  ( $=\mu/\rho$ ), Reynolds number ( $Re$ ) and Nusselt number ( $Nu$ ) are characterized by Eqs. (9a-b).

$$Re = \frac{U_o d}{\nu^T} = \frac{\rho U_o d}{\mu^T} \quad Nu = \frac{hd}{\kappa_f^T} = \frac{\partial T / \partial r|_{r=R} d}{T_s - T_o} \quad (9a-b)$$

The temperature dependent character of water properties ( $\xi$ ) is widely known (Incropera & DeWitt, 2001) and the scientific need in implementing their variation with temperature stands as a must in computational work. Thus the water properties of specific heat ( $C_p$ ), kinematic viscosity and thermal conductivity are gathered (Incropera & DeWitt, 2001) and fitted into 6<sup>th</sup> order polynomials (Eq. (10)). As the superscript T denotes the temperature dependency, the peak uncertainty of 0.03% is realized in Eq. (10) for the complete set of properties.

$$\zeta_T = \sum_{j=0}^6 a_j T^j \quad (10)$$

Due to the existence of the velocity and temperature gradients in the flow volume, positive and finite volumetric entropy generation rate arises throughout the micropipe. In the guidance of the Gouy-Stodola theorem (Kotas et al., 1995), entropy generation can be considered to be directly proportional to the lost available work, which takes place as a result of the non-equilibrium phenomenon of exchange of energy and momentum within the fluid and at the solid boundaries.

For a one-dimensional flow and two-dimensional temperature domain for incompressible Newtonian fluid flow in cylindrical coordinates, the local rate of entropy generation per unit volume ( $S'''$ ) can be calculated by Eq. (11a), where the temperature dependent character of both the thermal conductivity and the kinematic viscosity of water are as well taken into consideration. As the first term on the right side of Eq. (11a) stands for the local entropy generation due to finite temperature differences ( $S'''_{\Delta T}$ ) in axial  $z$  and in radial  $r$  directions, the local frictional entropy generation ( $S'''_{\Delta P}$ ) is defined by the second term. The input data, for either of the open (Eq. (11a)) or closed form (Eq. (11b)) illustrations of  $S'''$ , are attained by the computation of the temperature and the velocity fields through Eqs. (2-4).

$$S''' = \frac{k_f^T}{T^2} \left[ \left( \frac{\partial T}{\partial r} \right)^2 + \left( \frac{\partial T}{\partial z} \right)^2 \right] + \frac{\mu^T}{T} \left[ \left( \frac{\partial U_z}{\partial r} \right)^2 \right] \quad S''' = S'''_{\Delta T} + S'''_{\Delta P} \quad (11a-b)$$

Eqs. (12a-c) stand for the cross-sectional thermal ( $S'_{\Delta T}$ ), frictional ( $S'_{\Delta P}$ ) and total ( $S'$ ) entropy generation rates, where the common method is the integration of the local values over the cross-sectional area of the micropipe.

$$S'_{\Delta T} = 2\pi \int_{r=0}^{r=R} S'''_{\Delta T} r dr \quad S'_{\Delta P} = 2\pi \int_{r=0}^{r=R} S'''_{\Delta P} r dr \quad S' = 2\pi \int_{r=0}^{r=R} S''' r dr \quad (12a-c)$$

Bejan number is defined as the ratio of the thermal entropy generation to the total value. The cross-sectional average value of  $Be$  is given by Eq. (13).

$$Be = \frac{S'_{\Delta T}}{S'} \quad (13)$$

Not only to identify the shift of the determined fluid motion and heat transfer characteristics from the conventional theory but also to spot the individual and combined roles of  $\epsilon$ ,  $d$  and  $Re$  on the transition mechanism, the basic theoretical equations are as well incorporated in the formulation set. The shift of the velocity profiles from the characteristic styles of laminar and turbulent regimes can be enlightened through comparisons with the classical laminar velocity profile and the modified turbulent logarithm law for roughness (Eqs. (14a-b)) (White, 1999).

$$\frac{U(r)}{U_o} = 2 \left[ 1 - \left( \frac{r}{R} \right)^2 \right] \quad \frac{U(r)}{\sqrt{\tau_w / \rho}} = 2.44 \ln \left( \frac{R-r}{\epsilon} \right) + 8.5 \quad (14a-b)$$

The laminar temperature profile formula for Constant Heat Flux (CHF) applications is given by Eq. (15) (Incropera & DeWitt, 2001).

$$T(r) = T_s - \frac{2U_o K_f^T R^2}{\rho C_p^T} \left( \frac{dT_o}{dz} \right) \left[ \frac{3}{16} + \frac{1}{16} \left( \frac{r}{R} \right)^4 - \frac{1}{4} \left( \frac{r}{R} \right)^2 \right] \quad (15)$$

Boundary layer parameters like shape factor ( $H$ ) (Eq. (16a)) and intermittency ( $\gamma$ ) (Eq. (16b)) (White, 1999) are integrated into the discussions to strengthen the evaluations on the onset of transition, where  $U_c$  stands for the velocity at the pipe centerline. As the laminar ( $H_{lam}=3.36$ ) and turbulent ( $H_{turb}=1.70$ ) shape factor values are computed with Eq. (16a), by integrating the laminar (Eq. (14a)) and turbulent (Eq. (14b)) profiles, the shape factor data of the transitional flows were also calculated with Eq. (16a), however with the computationally evaluated corresponding velocity profiles.

$$H = \frac{\int_{r=0}^{r=R} \left( 1 - \frac{U(r)}{U_c} \right) r dr}{\int_{r=0}^{r=R} \frac{U(r)}{U_c} \left( 1 - \frac{U(r)}{U_c} \right) r dr} \quad \gamma = \frac{H_{lam} - H}{H_{lam} - H_{turb}} \quad (16a-b)$$

To clarify the role of surface roughness on the frictional activity, the classical and normalized friction coefficient values are evaluated by Eqs. (17a-c) (White, 1999).

$$C_f = \frac{2\mu^T \left| \frac{dU}{dr} \right|_{r=R}}{\rho_o U_o^2} \quad (C_f)_{lam} = \frac{16}{Re} \quad C_f^* = \frac{C_f}{(C_f)_{lam}} \quad (17a-c)$$

Viscous power loss ( $\Omega_{loss}$ ) per unit volume is the last term on the right hand side of the energy equation (Eq. (4)). Due to incompressibility, velocity does not vary in the streamwise direction ( $\partial U_z / \partial z = 0$ ); thus the viscous power loss data can be evaluated by Eq. (18).

$$\Omega_{loss} = 2\pi \int_{z=0}^{z=L} \int_{r=0}^{r=R} U_z(r) \frac{1}{r} \frac{\partial}{\partial r} (r\tau_{rz}) r dr dz \quad (18)$$

### 2.3 Computational technique

To ensure that the obtained solutions are independent of the grid employed and to examine the fineness of the computational grids, the flow domain of Fig. 1(a) is divided into  $m$  axial and  $n$  radial cells ( $m \times n$ ) and a series of successive runs, to fix the optimum axial and radial cell numbers, are performed. Preliminary test analyses pointed out the best possible cell orientation as  $m=500 \rightarrow 850$  and  $n=100 \rightarrow 225$  respectively, for  $d=1.00 \rightarrow 0.50$  mm. In the two-dimensional marching procedure, the axial and radial directions are scanned with forward difference discretization. To promote the computational capabilities and to enhance the concurrent interaction of the fluid flow, momentum structure and energy transfer (Eqs. (2-4)) characteristics of the considered scenario frame, the converted explicit forms of the principle equations are accumulated into the three-dimensional "Transfer Matrix". To

sensitively compute the velocity and temperature gradients on the pipe walls, the 20% of the radial region, neighboring the solid wall, is employed an adaptive meshing with radial-mesh width aspect ratio of  $1.1 \rightarrow 1.05$  ( $d=1.00 \rightarrow 0.50$  mm). The influences of surface roughness and surface heat flux conditions, over the meshing intervals of the flow domain, are coupled by Direct Simulation Monte Carlo (DSMC) method. DSMC method, as applied by Wu & Tseng (2001) to a micro-scale flow domain, is a utilized technique especially for internal flow applications. DSMC method can couple the influences of surface roughness and surface heat flux conditions over the meshing intervals of the flow domain. The benefits become apparent when either the initial guesses on inlet pressure and inlet velocity do not result in convergence within the implemented mesh, or if the converged solution does not point out the desired Reynolds number in the pipe. The "Transfer Matrix" scheme and the DSMC algorithm are supported by cell-by-cell transport tracing technique to guarantee mass conservation, boundary pressure matching and thermal equilibrium within the complete mesh. For accurate simulation of the inlet/exit pressure boundaries and additionally to sensitively evaluate the energy transferred in the flow direction, in the form of heat swept from the micropipe walls, the concept of triple transport conservation is as well incorporated into the DSMC. Newton-Raphson method is employed in the solution procedure of the resulting nonlinear system of equations, where the convergence criterion is selected as  $1 \times 10^{-7}$  for each parameter in the solution domain. By modifying the inlet pressure and temperature, DSMC algorithm activates to regulate the Reynolds number of the former iteration step, if the Reynolds number does not attain the objective level.

### 3. Results and discussion

The present research is carried out with the wide ranges of Reynolds number ( $Re=10-2000$ ), micropipe diameter ( $d=0.50-1.00$  mm), non-dimensional surface roughness ( $\epsilon^*=0.001-0.01$ ) and wall heat flux ( $q''=1000-2000$  W/m<sup>2</sup>) values, which in return creates the scientific platform not only to investigate their simultaneous and incorporated affects but also to identify the highlights and primary concerns of the fluid mechanics, heat transfer and thermodynamic issues of laminar-transitional micropipe flows. The considered micropipe diameter range is consistent with the micro-channel definition of Obot (2002) ( $d \leq 1.00$  mm). The length of the micropipe ( $L=0.5$  m), inlet temperature ( $T_{in}=278$  K) and exit pressure ( $P_{ex}=0$  Pa) of water flow are kept fixed throughout the analyses. The non-dimensional surface roughness range is in harmony with those of Engin et al. (2004) ( $\epsilon^* \leq 0.08$ ). On the other hand, to bring about applicable and rational heating, the imposed wall heat flux values are decided in conjunction with the Reynolds number and the accompanying mass flow rate ranges. Fluid mechanics issues are interpreted with radial velocity profiles, boundary layer parameters, friction coefficients, frictional power loss values. Issues on heat transfer are displayed by radial profiles of temperature and Nusselt numbers. Thermodynamic concepts are discussed in terms of the cross-sectional thermal, frictional and total entropy generation values and Bejan numbers. Scientific associations of the fluid mechanics, heat transfer and thermodynamic issues are also identified.

#### 3.1 Fluid mechanics issues

Issues on fluid mechanics are mainly related to the momentum characteristics of the micropipe flow and they are demonstrated by radial distributions of axial velocity profiles (VP) (Fig. 2), boundary layer parameters (Fig. 3), normalized friction coefficients ( $C_f^*$ ) (Fig. 4)



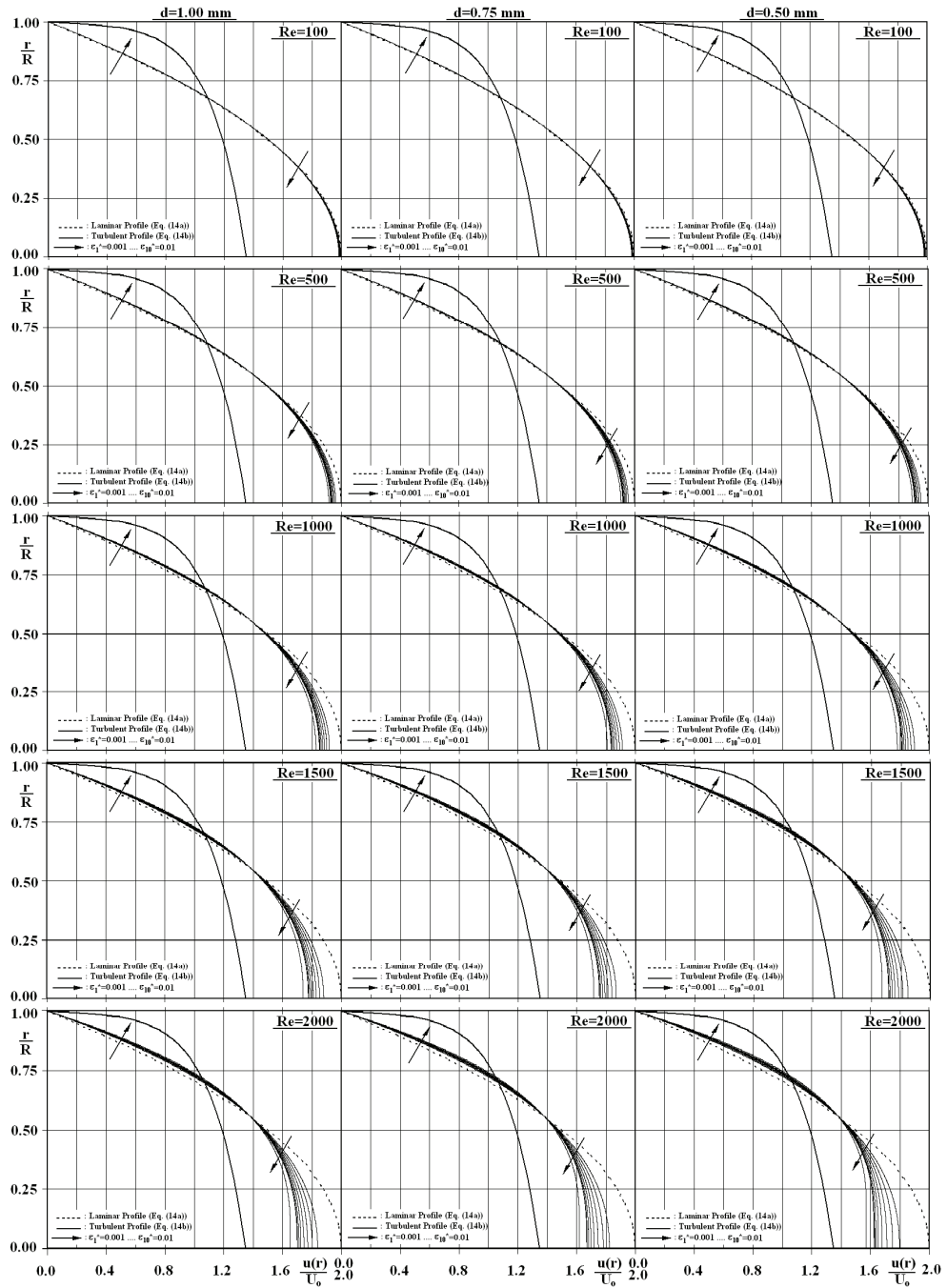


Fig. 2. Variation of radial distributions of axial velocity with  $Re$ ,  $d$  and  $\epsilon^*$

and power loss ( $\Omega_{loss}$ ) (Fig. 5) values. Computations indicated that surface heat flux had no affect on VP distribution, hydrodynamic boundary layer development,  $C_f^*$  and  $\Omega_{loss}$  variations; thus the representative plots (Figs. 2-5) clarify the combined roles of wall roughness ( $\epsilon$ ), micropipe diameter ( $d$ ) and Reynolds number ( $Re$ ) on the momentum characteristics of laminar-transitional flow. The radial distributions of axial velocity for the micropipe diameters of  $d=1.00, 0.75, 0.50$  mm, for the Reynolds numbers of  $Re=100, 500, 1000, 1500, 2000$  and for the non-dimensional surface roughness range of  $\epsilon^*=0.001-0.01$  is shown in Fig. 2. In the complete  $\epsilon^*$  and  $d$  ranges taken into consideration, the VPs of the  $Re=100$  scenario shown no sensible shift from the characteristic laminar profile (Eq. (14a)); where the corresponding boundary layer parameters (Fig. 3) show only slight deviations from the characteristic laminar data. As the shape factor and intermittency for the micropipe with  $d=1.00$  mm are calculated as  $H=3.347 \rightarrow 3.331$  &  $\gamma=0.008 \rightarrow 0.018$  ( $\epsilon^*=0.001 \rightarrow 0.01$ ), those of  $d=0.75$  mm come out to be  $H=3.346 \rightarrow 3.328$  &  $\gamma=0.009 \rightarrow 0.019$  and for  $d=0.50$  mm they become  $H=3.344 \rightarrow 3.324$  &  $\gamma=0.010 \rightarrow 0.022$ . Friction coefficient based viscous behavior of the flow is significant owing to its straight interrelation with the generation of frictional entropy (Eq. 11). As displayed in Fig. 4, higher surface roughness values elevates the frictional actions in micropipe flows, such that at the low Reynolds number of at  $Re=100$ , the rise of  $\epsilon^*$  from 0.001 to 0.01 manipulates the  $C_f^*$  to grow by  $\sim 0.7\%$  and  $\sim 0.9\%$  for the micropipes with  $d=1.00$  mm and  $d=0.50$  mm respectively. Velocity profiles are more apparently affected by roughness and diameter at higher Reynolds numbers (Fig. 2).

The lowest surface roughness of  $\epsilon^*=0.001$  result in, although poorer but identifiable, variations in the flow domain at  $Re=500$ , where the impact becomes more detectable at lower  $d$  with the interpreting data of  $H=3.291 \rightarrow 3.273$  &  $\gamma=0.042 \rightarrow 0.052$  ( $d=1.00 \rightarrow 0.50$  mm) (Fig. 3). The response of friction coefficient, to elevated surface roughness, becomes as well more rational at higher  $Re$ ; more particular indicating puts forward that as  $C_f^*$  is evaluated as  $1.006 \rightarrow 1.013$  ( $\epsilon^*=0.001 \rightarrow 0.01$ ),  $1.030 \rightarrow 1.065$  and  $1.091 \rightarrow 1.195$  for  $Re=100, 500$  and  $1500$  respectively at  $d=1.00$  mm, the corresponding values rise to  $C_f^*=1.008 \rightarrow 1.016, 1.038 \rightarrow 1.082$  and  $1.114 \rightarrow 1.246$  at  $d=0.50$  mm. The growing impact of surface roughness on friction coefficient at higher Reynolds numbers and lower micropipe diameters can evidently be inspected from these figures. Similar to the present findings, the augmenting role of roughness on friction coefficient with Reynolds number was as well documented by Vicente et al. (2002), Guo & Li (2003), Engin et al. (2004), Wang et al. (2005), Petropoulos et al. (2010) and Almeida et al. (2010).

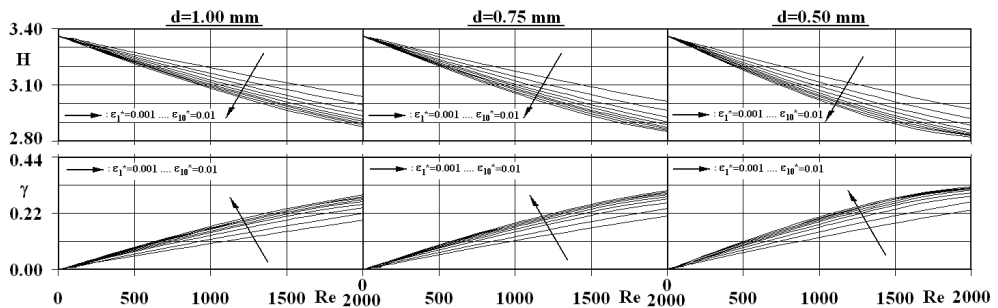


Fig. 3. Variation of  $H$  and  $\gamma$  with  $Re, d$  and  $\epsilon^*$

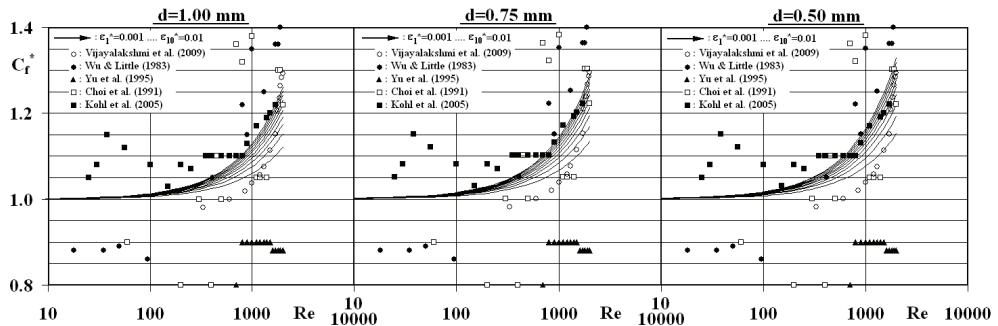


Fig. 4. Variation of  $C_f^*$  with  $Re$ ,  $d$  and  $\epsilon^*$

On the other hand, with the increase of Reynolds number the variation rates in  $C_f$  at different micropipe diameter cases, become stronger with the particular values of 3.4→4.2% ( $d=1.00\rightarrow 0.50$  mm), 6.6→8.1%, 9.6→11.9% and 12.4→15.2% for  $Re=500, 1000, 1500$  and  $2000$ . Renaud et al. (2008), Almeida et al. (2010) and Parlak et al. (2011) also shown the grow of frictional activity in micropipes with lower diameters. As shown in Fig. 4, as the experimental records of Yu et al. (1995) were below the laminar theory for  $100 < Re < 2000$ , Wu & Little (1983), Choi et al. (1991) and Kohl et al. (2005) also experimentally determined elevated friction coefficients for  $Re > 500$ . Moreover, in the particular surface roughness case of  $\epsilon^* = 0.002$ , comparably sharper increase rates in  $C_f^*$  for  $Re > 700$ , were experimentally recorded by Vijayalakshmi et al. (2009). The growing influence of surface roughness on the flow pattern (VPs) with lower micropipe diameter and higher Reynolds number is also demonstrated in Fig. 2. At higher  $\epsilon^*$  and  $Re$  and at lower  $d$ , the gap between the  $U_c/U_o$  ratios and the traditional data of  $U_c/U_o = 2.0$  (Eq. (14a)) increases. In addition to these, transition phenomena has been in the research agenda of several scientists and associating the augmentation of friction coefficient with the transition onset has become a tradition. Several researchers (Wu & Little, 1983, Obot, 2002, Vicente et al., 2002, Guo & Li, 2003, Kandlikar et al., 2003), performing experimental and numerical studies, recognized a 10% rise in  $C_f$  ( $C_f^* = 1.1$ ), above the traditional laminar formula of Eq. (17b), as an indicator for the transitional activity. The present computations pointed out that the laminar character continued up to the Reynolds number of  $Re = 600$  for the complete micropipe diameter ( $d = 1.00 - 0.50$  mm) and non-dimensional surface roughness ( $\epsilon^* = 0.001 - 0.01$ ) ranges considered with  $C_f^*$  values being lower than 1.1. The transitional Reynolds numbers appear as  $Re_{tra} \approx 1656 \rightarrow 769$  ( $\epsilon^* = 0.001 \rightarrow 0.01$ ),  $1491 \rightarrow 699$  and  $1272 \rightarrow 611$  for  $d = 1.00, 0.75$  and  $0.50$  mm, indicating the crucial authority of surface roughness on the transition process. These results clearly identify that micropipe diameter and roughness accelerates transition to lower Reynolds numbers. At the transition onset, the boundary layer approach (Eqs. (16a-b)) puts forward that the transitional shape factor and intermittency values appear in the contracted intervals of  $H = 3.135 - 3.142$  and  $\gamma = 0.132 - 0.135$  (Fig. 3). These ranges not only put forward that as shape factor falls, intermittency rises in due course of the shift from laminar character but also suggest the suitability of determining the transition onset by solely evaluating the intermittency information; in the current study  $\gamma \approx 0.135$  appears as the marker datum. It can be concluded with implicit trust that the decrease of  $H$  and  $U_c/U_o$  and the

complementary increase of  $C_f^*$  and  $\gamma$  are scientifically dependable indicators for the early stages of transitional activity in the fluid domain in micropipe flows. Besides, the present findings on the transitional Reynolds numbers are scientifically analogous with those of Wu & Little (1983) (for a range of  $\epsilon^* \Rightarrow Re_{tra} \approx 510-1170$ ), Obot (2002) (smooth pipe  $\Rightarrow Re_{tra} \approx 2040$ ) and Kandlikar et al. (2003) (for  $\epsilon^* \approx 0.003 \Rightarrow Re_{tra} \approx 1700$ ).

The concept of power loss ( $\Omega_{loss}$ ) can be considered as not only a terminological but also a scientific link among the frictional activity and the 2<sup>nd</sup> law characteristics of micropipe flows; thus the individual and combined actions of  $Re$ ,  $d$  and  $\epsilon^*$  on  $\Omega_{loss}$  and the so occurring deviations are presented in Fig. 5. It can clearly be inspected from the figure that power loss values grow with Reynolds number. Computations more explicitly defined that, the partial derivative of  $\partial\Omega_{loss} / \partial Re$  comes out to be  $5.34 \rightarrow 1.33$  ( $d=0.50 \rightarrow 1.00$  mm),  $10.8 \rightarrow 2.69$  and  $21.8 \rightarrow 5.40$  ( $\times 10^{-5}$ ) at the Reynolds numbers of  $Re=500$ ,  $1000$  and  $2000$  respectively. These numbers not only identify the non-linear dependence among  $\Omega_{loss}$  and  $Re$  but also the rapid grow of  $\Omega_{loss}$  with higher  $Re$  and with lower  $d$ , where the advanced micro attitude of the pipe diameter appears to more dominantly characterize this interaction at elevated Reynolds numbers. Fig. 5 additionally reveals that  $\Omega_{loss}$  gets the most remarkable values at the lowest micropipe diameter case of  $d=0.50$  mm, which can be attributed to the stronger frictional activity and the consequently enhanced viscous shear stress ( $\tau_{rz}$ ) values in the lower micropipe diameter scenarios with higher surface roughness (Fig. 4). Power loss due to friction in laminar flow was as well determined and reported by Koo & Kleinstreuer (2004), Morini (2005) and Celata et al. (2006a,b). Being completely in harmony with the present evaluations on the power loss mechanism, their computational and experimental findings not only exposed exponential augmentations in  $\Omega_{loss}$  due to high  $Re$  but also pointed out the direct relation of viscous dissipation with Reynolds number.

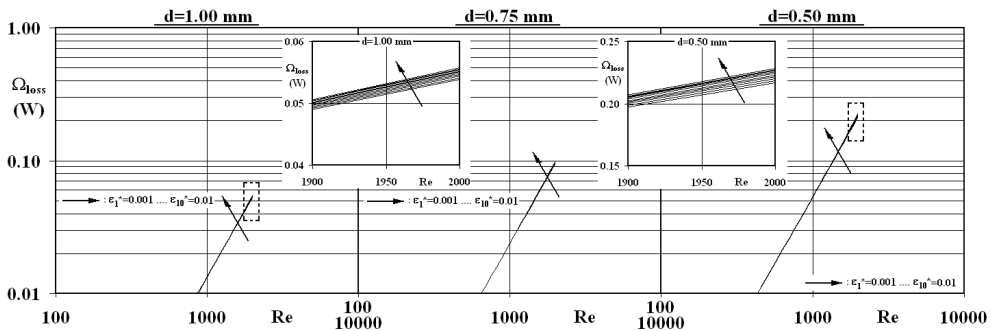


Fig. 5. Variation of  $\Omega_{loss}$  with  $Re$ ,  $d$  and  $\epsilon^*$

The zoomed plots for the micropipe diameter cases of  $d=1.00$  &  $0.50$  mm demonstrate additional information regarding the motivation of power loss values with surface roughness. Through comparisons among the scenario based computational outputs, the mechanism can be detailed with scientific accountability. The power loss values of the limiting surface roughness cases are reviewed with  $\Omega_{loss\epsilon^*=0.01} / \Omega_{loss\epsilon^*=0.001}$ , which results in

the ratios of 1.002→1.004 ( $d=1.00\rightarrow 0.50$  mm), 1.009→1.014 and 1.035→1.055 at the Reynolds numbers of  $Re=500, 1000$  and  $2000$  respectively. The growing action of surface roughness on power loss with lower micropipe diameter and higher Reynolds number can clearly be seen from these numbers.

### 3.2 Heat transfer issues

The primary consequence of the transfer of energy to fluid flow comes into sight through the response of the thermal structure, namely the temperature profile (TP) development, of the concept domain. Since the momentum and energy mechanisms considerably interact, the applied wall heat flux and viscous dissipation based energy loss ( $\Omega_{\text{loss}}$ ) on the solid walls simultaneously and strongly affect the TP in the fluid domain. Due to these facts and not only to identify the individual and combined roles of Reynolds number, micropipe diameter, surface roughness and heat flux on the thermal features of micropipe flows but also to display the deviation of the evaluated characteristics from the traditional laminar layout, Fig. 6 covers the TPs of various scenarios in conjunction with the laminar Constant Heat Flux (CHF) formula of Eq. (15) (Incropera & DeWitt, 2001). The figure shows that, in the complete  $Re$  and  $\epsilon^*$  cases taken into consideration, the TP of the micropipe with  $d=1.00$  mm are almost identical. The independent nature of the TPs from  $\epsilon^*$  can as well be identified through the non-dimensional temperature gradients (ndTG) on the pipe-surface  $\left(\left(\frac{\partial T}{\partial r}\right)_{r=R}\right)$ . Such that, as the ndTG of the Reynolds number cases of  $Re=500, 1000$  and  $2000$  get the values of  $ndTG=6.01, 5.99,$  and  $5.91$  ( $\times 10^{-3}$ ) at the highest heat flux level of  $2000$   $W/m^2$ , they drop down to  $ndTG=3.00, 2.98$  and  $2.90$  ( $\times 10^{-3}$ ) at the lowest level of  $1000$   $W/m^2$ .

There exists almost a two times gap among the ndTG values of the limiting heat flux applications, where the grow of the ndTG with  $q''$  can also be recognized as a result of enhanced heat addition on the walls of the thermal system. However, due to the promoted power loss values (Fig. 5) in the scenarios with higher  $Re$  and  $\epsilon^*$  and lower  $d$ , the comparison of the ndTGs among the limiting heat flux scenarios at  $d=0.50$  mm bring about the ratios of  $\left(\frac{\partial T}{\partial r}\right)_{r=R, q''=2000 W/m^2} / \left(\frac{\partial T}{\partial r}\right)_{r=R, q''=1000 W/m^2} \approx 2.00$  ( $Re=500$ ),  $\sim 2.08$  ( $Re=1000$ ) and  $\sim 2.37$  ( $Re=2000$ ), evidently pointing out the synergy of  $Re$  on the affects of  $q''$  on ndTG. On the other hand, ndTGs are evaluated to become moderate with the increase of mass flow rate, more specifically with Reynolds number, depending on the promoted competence of energy embracing in those scenarios. Computations put forward that the impact of surface roughness on the TP development becomes stronger at lower micropipe diameters, more explicitly with micro-activity. For the lowest diameter of  $d=0.50$  mm and at the highest heat flux condition of  $q''=2000$   $W/m^2$ , the plotted styles in Fig. 6 clarify that in the Reynolds number cases  $Re=500, 1000$  and  $2000$  ndTG attains the values of  $2.93\rightarrow 2.98$  ( $\times 10^{-3}$ ) ( $\epsilon^*=0.001\rightarrow 0.01$ ),  $2.82\rightarrow 2.91$  ( $\times 10^{-3}$ ) and  $2.31\rightarrow 2.59$  ( $\times 10^{-3}$ ) respectively. In the heat flux application of  $q''=1000$   $W/m^2$ , these gradients decrease down to  $ndTG=1.47\rightarrow 1.48$  ( $\times 10^{-3}$ ),  $1.36\rightarrow 1.40$  ( $\times 10^{-3}$ ) and  $0.98\rightarrow 1.09$  ( $\times 10^{-3}$ ) at the identical Reynolds numbers. The increase of the ndTG with  $\epsilon^*$  is an evidence of the augmenting role surface roughness on heat transfer.

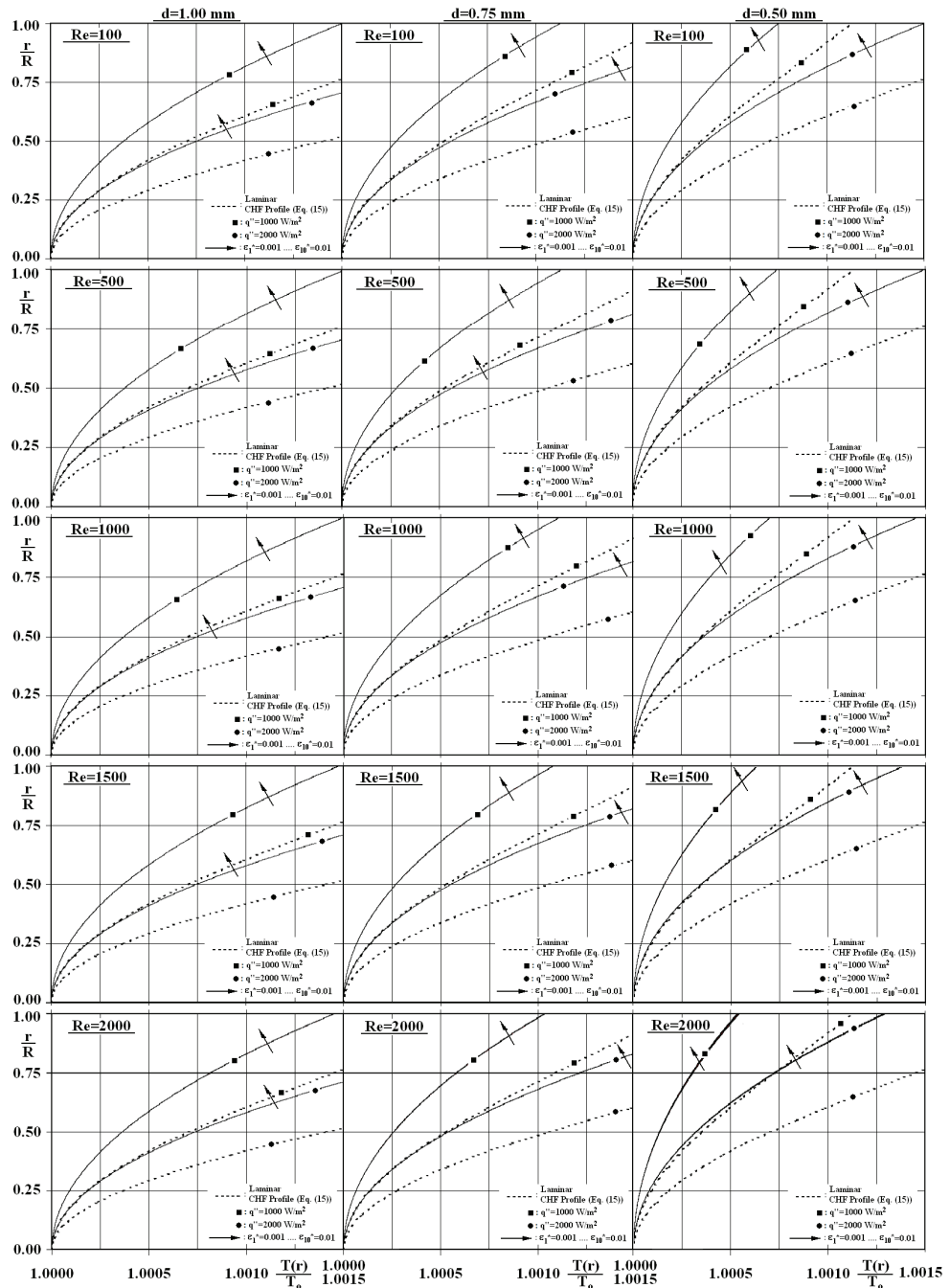


Fig. 6. Variation of radial distributions of temperature with  $Re, d, \epsilon^*$  and  $q''$

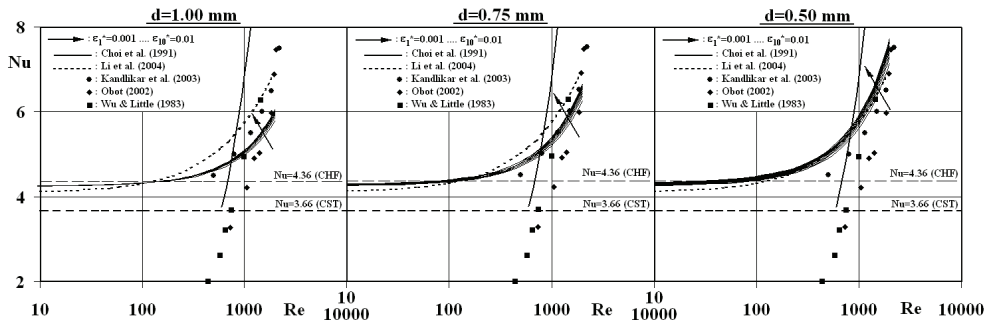


Fig. 7. Variation of Nu with Re, d and  $\epsilon^*$

Figure 7 displays the variation of Nusselt number with Reynolds number for various micropipe diameter ( $d=1.00-0.50$  mm) and surface roughness ( $\epsilon^*=0.001-0.01$ ) alternatives; the custom criteria of constant surface temperature ( $Nu_{CST}=3.66$ ) and constant heat flux ( $Nu_{CHF}=4.36$ ) for laminar flow are as well supplied in the graph. Moreover, the empiric equation of Choi et al. (1991) (Eq. (19a)) and Li et al.'s (2004) analogy (Eq. (19b)) are also plotted for comparison purposes.

$$Nu = 0.0000972 * Re^{1.17} * Pr^{0.333} \quad Nu = 4.1 + \frac{0.14*d/L*Re*Pr}{1 + 0.05*(d/L*Re*Pr)^{2/3}} \quad (19a-b)$$

Computations indicated an almost constant Nusselt number of  $Nu=4.25$  for  $Re \leq 100$  in the complete micropipe diameter and surface roughness ranges; Vicente et al. (2002) as well reported for  $Re < 700$  that Nusselt number remained stable around  $Nu \sim 4.36$ . The present outcome is not only analogous with the traditional laminar values of  $Nu_{CST}$  and  $Nu_{CHF}$  but also identifies the thermally ineffective presence of the  $d$  and  $\epsilon^*$ . Above  $Re=100$ , heat transfer rates are motivated by flow velocity such that Nusselt numbers determined to increase with Reynolds number. Particularly it can more easily be clarified for the  $d=1.00$  mm case that the roughness range ( $\epsilon^*=0.001-0.01$ ) based average  $Nu_{Re=100}/Nu_{Re=10}$ ,  $Nu_{Re=500}/Nu_{Re=100}$ ,  $Nu_{Re=1000}/Nu_{Re=500}$  and  $Nu_{Re=2000}/Nu_{Re=1000}$  ratios attain the values of 1.016, 1.073, 1.090 and 1.180, where these figures become 1.021→1.030, 1.094→1.133, 1.114→1.156 and 1.223→1.294 for  $d=0.75 \rightarrow 0.50$  mm. These figures clearly identify that the heat transfer mechanism is subjected to the non-linear and also concurrently growing influence of Reynolds number with the micropipe diameter. Choi et al. (1991), Obot (2002), Vicente et al. (2002) and Li et al. (2004) also recorded elevated heat transfer rates with Reynolds number. As the empiric equation (Eq. (19a)) of Choi et al. (1991) matches with the present outputs only in the narrow Reynolds number band of  $700 < Re < 900$ , the analogy (Eq. (19b)) of Li et al. (2004) resemble similar outputs with the current evaluations in the Reynolds number range of  $Re > 300$  for the micropipes with the diameters of  $d=0.50-0.75$  mm. Moreover, the experimental data of Wu & Little (1983) (for  $Re \geq 1000$ ), Obot (2002) (for  $Re \geq 1000$ ) and Kandlikar et al. (2003) (for  $Re \geq 500$ ) are reasonably in harmony with the current numerical outputs. Figure 7 further demonstrates the enhancing function surface roughness on Nusselt number, where Wu & Cheng (2003) and Kandlikar et al.

(2003) also notified the rise of heat transfer rates with surface roughness through their experimental works. The present calculations further denoted the rising impact of surface roughness on Nusselt number at lower micropipe diameters and higher Reynolds numbers. It can more particularly be clarified that, at the lowest micropipe diameter case of  $d=0.50$  mm, the  $Nu_{\epsilon^*=0.01}/Nu_{\epsilon^*=0.001}$  ratio attains the values of 1.023 (Re=100), 1.039 (Re=500), 1.056 (Re=1000) and 1.082 (Re=2000), whereas the proportions become 1.011, 1.026, 1.040 and 1.062 for  $d=0.75$  and 1.002, 1.012, 1.025 and 1.046 for  $d=1.00$  mm. On the other hand, the influence of the transition mechanism on the heat transfer rates can be signified through comparisons among the Nu values ( $Nu_{tra}$ ) computed at  $Re_{tra}$  and the laminar value ( $Nu_{lam}=4.25$ ) attained at  $Re<100$ . The encouraged activity with the rates of 41.1→21.6% ( $\epsilon^*=0.001\rightarrow 0.01$ ) at  $d=0.50$  mm, 33.2→18.5% at  $d=0.75$  mm and 29.8→15.1% at  $d=1.00$  mm, designate that Nu at the transition onset grow by 1.22→1.15 ( $d=0.50\rightarrow 1.00$  mm) for  $\epsilon^*=0.01$  and by 1.41→1.30 for  $\epsilon^*=0.001$ . It can further be deduced from these evaluations that, the accelerated transition mechanism to considerably low  $Re_{tra}$  with higher surface roughness suppresses the thermal activity associated with transition; besides in fluid domains with lower micropipe diameters, the transitional heat transfer levels are encouraged with further synergy.

### 3.3 Thermodynamic issues

The concepts regarding the fluid mechanics and heat transfer mechanisms of micropipe flows are not only significant in their classified scientific research frame, but they are also recognizable due to their fundamental stance in developing the theoretical background for the thermodynamic investigations. Having identified the broad panorama of the momentum and thermal characteristics, the thermal, frictional and total entropy generation values and Bejan number can be outlined and discussed to interpret the thermodynamic issues and 2<sup>nd</sup> law mechanisms of micropipe flows.

Table 1 displays the variation of cross-sectional frictional entropy generation ( $S'_{\Delta P}$ ) values with various Reynolds number, micropipe diameter, surface roughness and surface heat flux scenarios. The tabulated values clearly identify for the complete ranges of Re, d and  $\epsilon^*$  that wall heat flux has almost no influence on frictional entropy generation, where this outcome can be associated with the identical VP formation in different heat flux applications (Fig. 2). Computations shown that microactivity, namely lower micropipe diameters, encourage the frictional entropy generation values; this finding can scientifically be interrelated with the augmentation of  $C_f^*$  data (Fig. 4) with lower d. Hooman (2008) as well perceived the growing role of lower micropipe diameter on frictional entropy generation rates. The individual and combined roles of the acting parameters on frictional entropy generation can scientifically be classified through the comparison strategy of  $S'_{\Delta P, d=0.50mm} / S'_{\Delta P, d=1.00mm}$ , which points out the complete surface heat flux range ( $q''=1000-2000$  W/m<sup>2</sup>) averaged ratios of 4.001→4.001 ( $\epsilon^*=0.001\rightarrow 0.01$ ), 4.002→4.007, 4.006→4.027 and 4.023→4.102 for Re=100, 500, 1000 and 2000 respectively. These figures clearly reveal that the surface roughness and micropipe diameter are augmenting factors on frictional entropy generation; moreover Reynolds number, or flow velocity, acts as a supporting-reagent on the impact of d and  $\epsilon^*$  on  $S'_{\Delta P}$ .



		$S'_{\Delta P}$ (W/mK) ( $\epsilon_1^*=0.001 \dots \epsilon_{10}^*=0.01$ )		
		$d=1.00$ mm	$d=0.75$ mm	$d=0.50$ mm
		$q''=1000$ W/m <sup>2</sup>	Re=100	9.58x10 <sup>-7</sup> ..... 9.58x10 <sup>-7</sup>
Re=500	2.40x10 <sup>-5</sup> ..... 2.40x10 <sup>-5</sup>		4.26x10 <sup>-5</sup> ..... 4.27x10 <sup>-5</sup>	9.59x10 <sup>-5</sup> ..... 9.62x10 <sup>-5</sup>
Re=1000	9.60x10 <sup>-5</sup> ..... 9.68x10 <sup>-5</sup>		1.71x10 <sup>-4</sup> ..... 1.72x10 <sup>-4</sup>	3.84x10 <sup>-4</sup> ..... 3.90x10 <sup>-4</sup>
Re=1500	2.17x10 <sup>-4</sup> ..... 2.21x10 <sup>-4</sup>		3.85x10 <sup>-4</sup> ..... 3.94x10 <sup>-4</sup>	8.69x10 <sup>-4</sup> ..... 8.96x10 <sup>-4</sup>
Re=2000	3.87x10 <sup>-4</sup> ..... 4.00x10 <sup>-4</sup>		6.89x10 <sup>-4</sup> ..... 7.17x10 <sup>-4</sup>	1.56x10 <sup>-3</sup> ..... 1.64x10 <sup>-3</sup>
$q''=2000$ W/m <sup>2</sup>	Re=100	9.57x10 <sup>-7</sup> ..... 9.57x10 <sup>-7</sup>	1.70x10 <sup>-6</sup> ..... 1.70x10 <sup>-6</sup>	3.83x10 <sup>-6</sup> ..... 3.83x10 <sup>-6</sup>
	Re=500	2.39x10 <sup>-5</sup> ..... 2.40x10 <sup>-5</sup>	4.26x10 <sup>-5</sup> ..... 4.27x10 <sup>-5</sup>	9.58x10 <sup>-5</sup> ..... 9.61x10 <sup>-5</sup>
	Re=1000	9.59x10 <sup>-5</sup> ..... 9.67x10 <sup>-5</sup>	1.71x10 <sup>-4</sup> ..... 1.72x10 <sup>-4</sup>	3.84x10 <sup>-4</sup> ..... 3.90x10 <sup>-4</sup>
	Re=1500	2.16x10 <sup>-4</sup> ..... 2.21x10 <sup>-4</sup>	3.85x10 <sup>-4</sup> ..... 3.94x10 <sup>-4</sup>	8.69x10 <sup>-4</sup> ..... 8.96x10 <sup>-4</sup>
	Re=2000	3.86x10 <sup>-4</sup> ..... 4.00x10 <sup>-4</sup>	6.88x10 <sup>-4</sup> ..... 7.17x10 <sup>-4</sup>	1.55x10 <sup>-3</sup> ..... 1.64x10 <sup>-3</sup>

Table 1. Variation of  $S'_{\Delta P}$  with Re, d,  $\epsilon^*$  and  $q''$

On the other hand,  $S'_{\Delta P}$  are investigated to increase with Re in the complete d range taken into consideration. The systematically gathered numerical outputs identified the linear variation of  $S'_{\Delta P}$  with Re on logarithmic scale. The analysis confirmed the exciting impact of lower d on the ascend of  $S'_{\Delta P}$  with Re, where the representative  $\partial \log S'_{\Delta P} / \partial \log Re$  ratios are evaluated as 2.012, 2.009 and 2.008 for d=0.50, 0.75 and 1.00 mm respectively. The tabulated values in Table 1 further exhibits that  $S'_{\Delta P}$  are also manipulated by  $\epsilon^*$ . The outputs of the limiting scenarios can be compared with the ratio of  $S'_{\Delta P}_{\epsilon^*=0.01} / S'_{\Delta P}_{\epsilon^*=0.001}$ , which results in the growing rates of 1.000→1.000 (Re=100) (d=1.00→0.50 mm), 1.002→1.003 (Re=500), 1.008→1.014 (Re=1000) and 1.034→1.055 (Re=2000). The evidently more definite impact of  $\epsilon^*$  on  $S'_{\Delta P}$  at higher Re and lower d can be noticed from these proof; however they must still be labelled as originated from the secondary-sort influence of surface roughness on frictional entropy.

The thermal distortions, in the fluid domain, or the strong temperature gradients, especially on the physical boundaries of the system, account for irreversibilities, which as a consequence cause the loss of available energy or the decrease of thermal efficiency. The defining scientific expression is widely accepted as the thermal entropy generation and it is also known to considerably interrelate with the levels of Re, d,  $\epsilon^*$  and  $q''$ . To identify the influential intensities of the acting operational components on the cross-sectional thermal entropy generation ( $S'_{\Delta T}$ ), Table 2 is structured. The temperature profile characteristics and the local values of temperature in the fluid domain can computationally (Eq. (11a)) be considered as the sources of  $S'_{\Delta T}$ ; however the previous discussions on T(r) (Fig. 6) clearly designated the significant manipulation capabilities of Reynolds number, micropipe diameter, surface roughness, and surface heat flux on TP development. The superior  $S'_{\Delta T}$  in

micropipes with larger diameters can be inspected from the tabulated data. As the scientific explanation can be interpreted through the stronger temperature gradients (Fig. 6) with higher  $d$ , numerical comparisons identify additional valuable information. In the highest heat flux application of  $q'' = 2000 \text{ W/m}^2$  the complete surface roughness range ( $\epsilon^* = 0.001 - 0.01$ ) averaged  $S'_{\Delta T_{d=1.00\text{mm}}} / S'_{\Delta T_{d=0.50\text{mm}}}$  ratio comes out to be 3.998 (Re=100), 4.056 (Re=500), 4.249 (Re=1000) and 5.241 (Re=2000); but they decrease down to 4.003, 4.120, 4.531 and 7.267 as the imposed flux is lowered to  $q'' = 1000 \text{ W/m}^2$ . These proportions clearly show that the physical measures in microflow systems can become comprehensively dominant on the thermal entropy generation characteristics especially with lower heat flux applications and in scenarios with higher flow velocity or mass flow rate. Table 2 additionally illustrates the encouraging attempts of  $q''$  on  $S'_{\Delta T}$ , which directly originates from the stronger temperature gradients. Computations indicated the  $S'_{\Delta T_{q''=2000\text{W/m}^2}} / S'_{\Delta T_{q''=1000\text{W/m}^2}}$  ratios of 3.996, 4.005, 4.031 and 4.142 at Re=100, 500, 1000 and 2000 for  $d=1.00 \text{ mm}$ ; whereas these figures rise to 3.998  $\rightarrow$  4.001, 4.017  $\rightarrow$  4.068, 4.080  $\rightarrow$  4.298 and 4.369  $\rightarrow$  5.743 for  $d=0.75 \rightarrow 0.50 \text{ mm}$ . These figures indicate the supporting action of lower  $d$  and higher Re on the  $q'' - S'_{\Delta T}$  interaction. From surface roughness point of view, the tabulated data summarize the almost insensible affects of  $\epsilon^*$  on  $S'_{\Delta T}$ , especially in the micropipes with  $d=1.00 \text{ mm}$  &  $0.75 \text{ mm}$ . Although very minor when compared to those of  $d$ , Re and  $q''$ , surface roughness comes out to evoke its potential on thermal entropy generation in the micropipe diameter case of  $d=0.50 \text{ mm}$  and only for  $\text{Re} \geq 1500$ . Computations revealed the most remarkable  $S'_{\Delta T}$  manipulations due to  $\epsilon^*$  in the scenario of  $\text{Re}=2000 - q'' = 1000 \text{ W/m}^2$ , where the  $S'_{\Delta T_{\epsilon^*=0.01}} / S'_{\Delta T_{\epsilon^*=0.001}}$  ratio come out as 1.044, 1.008 and 1.002 for  $d=0.50, 0.75$  and  $1.00 \text{ mm}$ .

		$S'_{\Delta T} \text{ (W/mK)} (\epsilon_1^* = 0.001 \dots \epsilon_{10}^* = 0.01)$		
		$d = 1.00 \text{ mm}$	$d = 0.75 \text{ mm}$	$d = 0.50 \text{ mm}$
		$q'' = 1000 \text{ W/m}^2$	<b>Re=100</b>	8.48x10 <sup>-6</sup> ..... 8.48x10 <sup>-6</sup>
<b>Re=500</b>	8.44x10 <sup>-6</sup> ..... 8.44x10 <sup>-6</sup>		4.72x10 <sup>-6</sup> ..... 4.72x10 <sup>-6</sup>	2.05x10 <sup>-6</sup> ..... 2.05x10 <sup>-6</sup>
<b>Re=1000</b>	8.33x10 <sup>-6</sup> ..... 8.33x10 <sup>-6</sup>		4.58x10 <sup>-6</sup> ..... 4.58x10 <sup>-6</sup>	1.84x10 <sup>-6</sup> ..... 1.84x10 <sup>-6</sup>
<b>Re=1500</b>	8.15x10 <sup>-6</sup> ..... 8.16x10 <sup>-6</sup>		4.34x10 <sup>-6</sup> ..... 4.34x10 <sup>-6</sup>	1.50x10 <sup>-6</sup> ..... 1.52x10 <sup>-6</sup>
<b>Re=2000</b>	7.89x10 <sup>-6</sup> ..... 7.91x10 <sup>-6</sup>		3.99x10 <sup>-6</sup> ..... 4.02x10 <sup>-6</sup>	1.07x10 <sup>-6</sup> ..... 1.11x10 <sup>-6</sup>
$q'' = 2000 \text{ W/m}^2$	<b>Re=100</b>	3.39x10 <sup>-5</sup> ..... 3.39x10 <sup>-5</sup>	1.91x10 <sup>-5</sup> ..... 1.91x10 <sup>-5</sup>	8.47x10 <sup>-6</sup> ..... 8.47x10 <sup>-6</sup>
	<b>Re=500</b>	3.38x10 <sup>-5</sup> ..... 3.38x10 <sup>-5</sup>	1.90x10 <sup>-5</sup> ..... 1.90x10 <sup>-5</sup>	8.33x10 <sup>-6</sup> ..... 8.33x10 <sup>-6</sup>
	<b>Re=1000</b>	3.36x10 <sup>-5</sup> ..... 3.36x10 <sup>-5</sup>	1.87x10 <sup>-5</sup> ..... 1.87x10 <sup>-5</sup>	7.90x10 <sup>-6</sup> ..... 7.91x10 <sup>-6</sup>
	<b>Re=1500</b>	3.32x10 <sup>-5</sup> ..... 3.32x10 <sup>-5</sup>	1.82x10 <sup>-5</sup> ..... 1.82x10 <sup>-5</sup>	7.18x10 <sup>-6</sup> ..... 7.22x10 <sup>-6</sup>
	<b>Re=2000</b>	3.27x10 <sup>-5</sup> ..... 3.27x10 <sup>-5</sup>	1.75x10 <sup>-5</sup> ..... 1.75x10 <sup>-5</sup>	6.19x10 <sup>-6</sup> ..... 6.30x10 <sup>-6</sup>

Table 2. Variation of  $S'_{\Delta T}$  with Re,  $d$ ,  $\epsilon^*$  and  $q''$

		$S' \text{ (W/mK)} (\epsilon_1^* = 0.001 \dots \epsilon_{10}^* = 0.01)$		
		$d = 1.00 \text{ mm}$	$d = 0.75 \text{ mm}$	$d = 0.50 \text{ mm}$
$q'' = 1000 \text{ W/m}^2$	<b>Re=100</b>	9.43x10 <sup>-6</sup> ..... 9.43x10 <sup>-6</sup>	6.47x10 <sup>-6</sup> ..... 6.47x10 <sup>-6</sup>	5.95x10 <sup>-6</sup> ..... 5.95x10 <sup>-6</sup>
	<b>Re=500</b>	3.24x10 <sup>-5</sup> ..... 3.24x10 <sup>-5</sup>	4.73x10 <sup>-5</sup> ..... 4.74x10 <sup>-5</sup>	9.79x10 <sup>-5</sup> ..... 9.82x10 <sup>-5</sup>
	<b>Re=1000</b>	1.04x10 <sup>-4</sup> ..... 1.05x10 <sup>-4</sup>	1.75x10 <sup>-4</sup> ..... 1.77x10 <sup>-4</sup>	3.86x10 <sup>-4</sup> ..... 3.92x10 <sup>-4</sup>
	<b>Re=1500</b>	2.25x10 <sup>-4</sup> ..... 2.29x10 <sup>-4</sup>	3.90x10 <sup>-4</sup> ..... 3.94x10 <sup>-4</sup>	8.71x10 <sup>-4</sup> ..... 8.79x10 <sup>-4</sup>
	<b>Re=2000</b>	3.94x10 <sup>-4</sup> ..... 4.08x10 <sup>-4</sup>	6.93x10 <sup>-4</sup> ..... 7.21x10 <sup>-4</sup>	1.56x10 <sup>-3</sup> ..... 1.64x10 <sup>-3</sup>
$q'' = 2000 \text{ W/m}^2$	<b>Re=100</b>	3.48x10 <sup>-5</sup> ..... 3.48x10 <sup>-5</sup>	2.08x10 <sup>-5</sup> ..... 2.08x10 <sup>-5</sup>	1.23x10 <sup>-5</sup> ..... 1.23x10 <sup>-5</sup>
	<b>Re=500</b>	5.77x10 <sup>-5</sup> ..... 5.78x10 <sup>-5</sup>	6.15x10 <sup>-5</sup> ..... 6.16x10 <sup>-5</sup>	1.04x10 <sup>-4</sup> ..... 1.04x10 <sup>-4</sup>
	<b>Re=1000</b>	1.30x10 <sup>-4</sup> ..... 1.30x10 <sup>-4</sup>	1.89x10 <sup>-4</sup> ..... 1.91x10 <sup>-4</sup>	3.92x10 <sup>-4</sup> ..... 3.97x10 <sup>-4</sup>
	<b>Re=1500</b>	2.50x10 <sup>-4</sup> ..... 2.54x10 <sup>-4</sup>	4.03x10 <sup>-4</sup> ..... 4.12x10 <sup>-4</sup>	8.76x10 <sup>-4</sup> ..... 9.03x10 <sup>-4</sup>
	<b>Re=2000</b>	4.19x10 <sup>-4</sup> ..... 4.32x10 <sup>-4</sup>	7.06x10 <sup>-4</sup> ..... 7.35x10 <sup>-4</sup>	1.56x10 <sup>-3</sup> ..... 1.65x10 <sup>-3</sup>

Table 3. Variation of  $S'$  with Re, d,  $\epsilon^*$  and  $q''$

Table 3 shows the individual and combined roles of Reynolds number, micropipe diameter, surface roughness and surface heat flux on the cross-sectional total entropy generation ( $S'$ ) values. Carrying out comparisons, among the limiting  $\epsilon^*$  cases, with  $S'_{\epsilon^*=0.01} / S'_{\epsilon^*=0.001}$  produced the deviation rates in the lowest micropipe diameter of  $d=0.50 \text{ mm}$  as  $1.000 \rightarrow 1.000$  ( $q'' = 1000 \rightarrow 2000 \text{ W/m}^2$ ) ( $Re=100$ ),  $1.003 \rightarrow 1.003$  ( $Re=500$ ),  $1.014 \rightarrow 1.013$  ( $Re=1000$ ) and  $1.055 \rightarrow 1.054$  ( $Re=2000$ ); indeed they further drop down to  $1.000 \rightarrow 1.000$ ,  $1.002 \rightarrow 1.001$ ,  $1.008 \rightarrow 1.006$  and  $1.034 \rightarrow 1.032$  in the micropipe with  $d=1.00 \text{ mm}$ . These records point out the insignificant affect of  $\epsilon^*$  on  $S'$ , which is analogous to its activity on  $S'_{\Delta P}$  and  $S'_{\Delta T}$ . Moreover, they propose that the influence rank of  $\epsilon^*$  on  $S'$  is similar to those of the corresponding findings for  $S'_{\Delta P}$  in the higher Reynolds number range, nevertheless resemble the  $S'_{\Delta T}$  scene in lower Reynolds number cases. On the other hand,  $S'$  are determined to rise with higher Re and  $q''$  and with lower d. The present evaluations can be detailed by the two fundamental reporting: Promoted total entropy generation (i) with low micropipe diameters and high fluid velocities is due to frictional entropy generation (Table 1), (ii) with the application of higher heat flux, bigger micropipe diameters and low Reynolds numbers count on thermal generation rates (Table 2). Enhanced entropy generation rates with higher Reynolds numbers and lower micropipe diameters are as well reported by Avci & Aydin (2007), Hooman (2008) and Parlak et al. (2011). In addition to the above determinations, through the ratio of  $S'_{q''=2000\text{W/m}^2} / S'_{q''=1000\text{W/m}^2}$  the magnitude of the influence of  $q''$  on  $S'$  is identified with the following comparison rates of  $3.692 \rightarrow 2.068$  ( $d=1.00 \rightarrow 0.50 \text{ mm}$ ) ( $Re=100$ ),  $1.782 \rightarrow 1.064$  ( $Re=500$ ),  $1.241 \rightarrow 1.015$  ( $Re=1000$ ) and  $1.061 \rightarrow 1.003$  ( $Re=2000$ ). The stronger influence potential of heat flux on total entropy generation with lower Reynolds numbers and higher micropipe

diameter can be inspected from these proportions. Table 3 as well presents for high Reynolds numbers the convergence of the  $S'$  with different  $q''$  levels, where at the lowest micropipe diameter scenario ( $d=0.50$  mm) the  $S'$  become approximately matching.

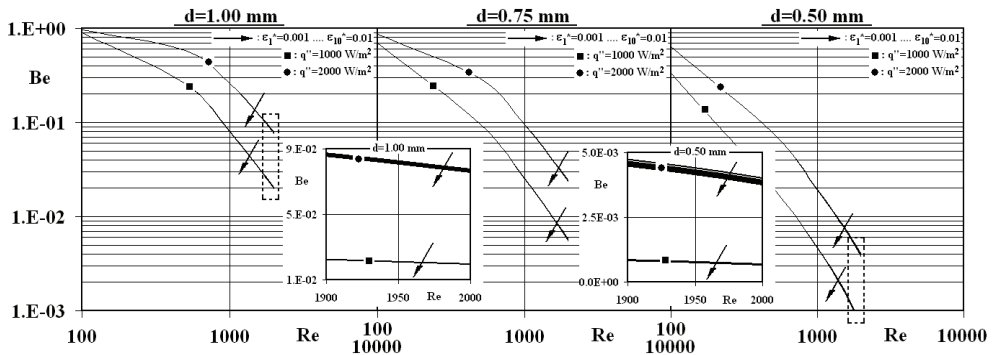


Fig. 8. Variation of Be with Re,  $d$ ,  $\epsilon^*$  and  $q''$

Variation of the cross-sectional average Bejan number (Be) with Reynolds number, micropipe diameter, surface roughness and wall heat flux in micropipe flows is exhibited in Fig. 8. The negligible influence of surface roughness on Bejan number can be clarified by comparing the Be of the limiting roughness cases. For the micropipe diameter of  $d=0.50$  mm the ratio of  $Be_{\epsilon^*=0.01}/Be_{\epsilon^*=0.001}$  is calculated as  $1.000 \rightarrow 1.000$  ( $q''=1000 \rightarrow 2000$  W/m<sup>2</sup>),  $0.997 \rightarrow 0.997$ ,  $0.985 \rightarrow 0.986$  and  $0.909 \rightarrow 0.932$  at  $Re=100, 500, 1000$  and  $2000$ , whereas these numbers rise to  $1.000 \rightarrow 1.000$ ,  $0.998 \rightarrow 0.998$ ,  $0.992 \rightarrow 0.994$  and  $0.965 \rightarrow 0.968$  for  $d=1.00$  mm. The growing treatment of  $\epsilon^*$  on Be with higher Re and lower  $q''$  and  $d$  is important from the point of both energy and exergy mechanisms of micropipe flows. On the other hand, due to the high  $S'_{\Delta T}$  values in higher  $q''$  intensities, Bejan number become superior in the corresponding scenarios. As  $Be=0.50$  stands for the identical  $S'_{\Delta T}$  and  $S'_{\Delta P}$  values, the emerging Reynolds number is as well significant from the point of energetic and exergetic issues of micropipe flows. Computations pointed out the  $Re_{Be=0.50}$  values of  $\sim 296 \rightarrow \sim 589$  ( $q''=1000 \rightarrow 2000$  W/m<sup>2</sup>),  $\sim 168 \rightarrow \sim 332$  and  $\sim 80 \rightarrow \sim 150$  for  $d=1.00, 0.75$  and  $0.50$  mm. These figures clearly identify the encouraging action of micro-structure on frictional entropy and motivating mechanism of heat flux on thermal entropy generation, where these outcomes are as well in harmony with the previous discussions through Tables 1-3. Numerical analysis supply additional information characterizing the influence of  $q''$  on Be in different Re and  $d$  cases. The  $Be_{q''=1000\text{W/m}^2}/Be_{q''=2000\text{W/m}^2}$  ratio represents the augmentation rates of  $0.924 \rightarrow 0.517$  ( $d=1.00 \rightarrow 0.50$  mm),  $0.445 \rightarrow 0.262$ ,  $0.308 \rightarrow 0.236$  and  $0.256 \rightarrow 0.175$  for  $Re=100, 500, 1000$  and  $2000$ , denoting the growing role of  $q''$  on Be in higher Re and lower  $d$ . Figure 8 as well displays the decrease trends of Be with Re in the complete micropipe diameter, surface roughness and heat flux ranges considered in the analyses. Computations revealed the promoted the impact of Reynolds number with higher heat flux applications and with

lower diameter micropipes. On the other hand, Bejan numbers of the cases with higher heat flux and micropipe diameter came out to be advanced when compared with those of the other. This evaluation can be described by the encouraged thermal activity with the application of high heat flux on the pipe walls and through the enhanced thermal entropy generation rates in micropipes with higher diameter.

#### 4. Conclusions

The scientific findings of a comprehensive computational investigation, focusing on the roughness induced forced convective laminar-transitional micropipe flows, is reported. In the numerical analyses, Reynolds number, micropipe diameter, surface roughness and wall heat flux are considered in wide ranges. In the computations, as the converted explicit forms of the principle equations are accumulated into the three-dimensional Transfer Matrix, the influences of surface roughness and surface heat flux conditions are coupled by DSMC method. The Transfer Matrix scheme and the DSMC algorithm are as well supported by cell-by-cell transport tracing technique. To develop a complete overview on the 1<sup>st</sup> and 2<sup>nd</sup> law characteristics of flows in micropipes, fluid mechanics, heat transfer and thermodynamic issues are presented and discussed in detail. Radial distributions of axial velocity, boundary layer parameters, friction coefficients and power loss data are presented to recognize the fluid motion based concepts. The outputs on heat transfer results are demonstrated with radial temperature profiles and Nusselt numbers. Thermodynamic notions are interpreted with thermal, frictional and total entropy generation values and Bejan number. Scientific associations among the fluid mechanics, heat transfer and thermodynamic issues are also displayed, identified and revealed with academic liability.

#### 5. Acknowledgement

This research is supported by the Research Fund of the University of Uludag through project number: M(U)-2009/35.

#### 6. References

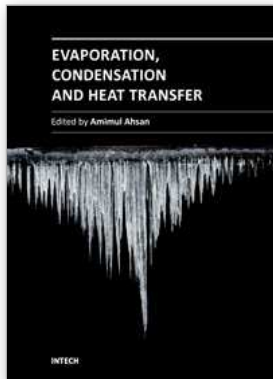
- Almeida, A.; Geraldies, V. & Semiao, V. (2010). Microflow Hydrodynamics in Slits: Effects of the Walls Relative Roughness and Spacer Inter-Filaments Distance. *Chemical Engineering Science*, Vol. 65, pp. 3660-3670, ISSN 0009-2509.
- Avci, M. & Aydin, O. (2007). Second-Law Analysis of Heat and Fluid Flow in Microscale Geometries. *International Journal of Exergy*, Vol. 4, pp. 286-301, ISSN 1742-8297.
- Cao, B.Y.; Chen, M. & Guo, Z.Y. (2006). Effect of Surface Roughness on Gas Flow in Microchannels by Molecular Dynamics Simulation. *International Journal of Engineering Science*, Vol. 44, pp. 927-937, ISSN 0020-7225.
- Celata, G.P.; Cumo, M.; McPhail, S. & Zummo, G. (2006a). Characterization of Fluid Dynamic Behaviour and Channel Wall Effects in Microtube. *International Journal of Heat and Fluid Flow*, Vol. 27, pp. 135-143, ISSN 0142-727X.
- Celata, G.P.; Morini, G.L.; Marconi, V.; McPhail, S.J. & Zummo, G. (2006b). Using Viscous Heating to Determine the Friction Factor in Microchannels - An Experimental Validation. *Experimental Thermal and Fluid Science*, Vol. 30, pp. 725-731, ISSN 0894-1777.

- Celata, G.P.; Lorenzini, M. & Morini, G.L. (2009). Friction Factor in Micropipe Gas Flow under Laminar, Transition and Turbulent Flow Regime. *International Journal of Heat and Fluid Flow*, Vol. 30, pp. 814-822, ISSN 0142-727X.
- Chen, S. & Tian, Z.W. (2010). Simulation of Thermal Micro-Flow using Lattice Boltzmann Method with Langmuir Slip Model. *International Journal of Heat and Fluid Flow*, Vol. 31, pp. 227-235, ISSN 0142-727X.
- Choi, S.B.; Barron, R.F. & Warrington, R.O. (1991). Fluid Flow and Heat Transfer in Microtubes. *Micromechanical Sensors, Actuators and Systems*, Vol. 32, pp. 123-134, ISSN 0924-4247.
- Engin, T.; Dogruer, U.; Evrensel, C.; Heavin, S. & Gordaninejad, F. (2004). Effect of Wall Roughness on Laminar Flow of Bingham Plastic Fluids through Microtubes. *Journal of Fluids Engineering - ASME Transactions*, Vol. 126, pp. 880-883, ISSN 0098-2202.
- Guo, Z.Y. & Li, Z.X. (2003). Size Effect on Microscale Single-Phase Flow and Heat Transfer. *International Journal of Heat and Mass Transfer*, Vol. 46, pp. 149-159, ISSN 0017-9310.
- Hooman, K. (2008). Heat Transfer and Entropy Generation for Forced Convection through a Microduct of Rectangular Cross-Section: Effects of Velocity Slip, Temperature Jump, and Duct Geometry. *International Communications in Heat and Mass Transfer*, Vol. 9, pp. 1065-1068, ISSN 0735-1933.
- Incropera, F.P. & DeWitt, D.P. (2001). *Fundamentals of Heat and Mass Transfer*, John Wiley & Sons, ISBN 9780471386506, New York.
- Kandlikar, S.G.; Joshi, S. & Tian, S. (2003). Effect of Surface Roughness on Heat Transfer and Fluid Flow Characteristics at Low Reynolds Numbers in Small Diameter Tubes. *Heat Transfer Engineering*, Vol. 24, pp. 4-16, ISSN 0145-7632.
- Ko, T.H. (2006a). Numerical Analysis of Entropy Generation and Optimal Reynolds Number for Developing Laminar Forced Convection in Double-Sine Ducts with Various Aspect Ratios. *International Journal of Heat and Mass Transfer*, Vol. 49, pp. 718-726, ISSN 0017-9310.
- Ko, T.H. (2006b). Numerical Investigation of Laminar Forced Convection and Entropy Generation in a Helical Coil with Constant Wall Heat Flux. *Numerical Heat Transfer Part-A*, Vol. 49, pp. 257-278, ISSN 1040-7782.
- Kohl, M.J.; Abdel-Khalik, S.I.; Jeter, S.M. & Sadowski, D.L. (2005). An Experimental Investigation of Microchannel Flow with Internal Pressure Measurements. *International Journal of Heat and Mass Transfer*, Vol. 48, pp. 1518-1533, ISSN 0017-9310.
- Koo, J. & Kleinstreuer, C. (2004). Viscous Dissipation Effects in Microtubes and Microchannels. *International Journal of Heat and Mass Transfer*, Vol. 47, pp. 3159-3169, ISSN 0017-9310.
- Kotas, T.J.; Mayhew, Y.R. & Raichura, R.C. (1995). Nomenclature for Exergy Analysis. *Proceedings of the Institution of Mechanical Engineers-Part A*, Vol. 209, pp. 275-280, ISSN 0263-7138.
- Li, J.; Peterson, G.P. & Cheng, P. (2004). Three-Dimensional Analysis of Heat Transfer in a Micro-Heat Sink with Single Phase Flow. *International Journal of Heat and Mass Transfer*, Vol. 47, pp. 4215-4231, ISSN 0017-9310.
- Morini, G.L. (2005). Viscous Heating in Liquid Flows in Micro-Channels. *International Journal of Heat and Mass Transfer*, Vol. 48, pp. 3637-3647, ISSN 0017-9310.

- Obot, N.T. (2002). Toward a Better Understanding of Friction and Heat/Mass Transfer in Microchannels - A Literature Review. *Microscale Thermophysical Engineering*, Vol. 6, pp. 155-173, ISSN 1089-3954.
- Ogedengbe, E.O.B.; Naterer, G.F. & Rosen, M.A. (2006). Slip Flow Irreversibility of Dissipative Kinetic and Internal Energy Exchange in Microchannels. *Journal of Micromechanics and Microengineering*, Vol. 16, pp. 2167-2176, ISSN 0960-1317.
- Ozgener, L.; Hepbasli, A. & Dincer, I. (2007). Parametric Study of the Effect of Reference State on Energy and Exergy Efficiencies of Geothermal District Heating Systems (GDHSs): An Application of the Salihli GDHS in Turkey. *Heat Transfer Engineering*, Vol. 28, pp. 357-364, ISSN 0145-7632.
- Parlak, N.; Gur, M.; Ari, V.; Kucuk, H. & Engin, T. (2011). Second Law Analysis of Water Flow through Smooth Microtubes under Adiabatic Conditions. *Experimental Thermal and Fluid Science*, Vol. 35, pp. 60-67, ISSN 0894-1777.
- Petropoulos, A.; Kaltsas, G. & Randjelovic, D. (2010). Study of Flow and Pressure Field in Microchannels with Various Cross-Section Areas. *Microelectronic Engineering*, Vol. 87, pp. 827-829, ISSN 0167-9317.
- Pitakarnnop, J.; Varoutis, S. & Valougeorgis, D. (2010). A Novel Experimental Setup for Gas Microflows. *Microfluidics and Nanofluidics*, Vol. 8, pp. 57-72, ISSN 1613-4982.
- Ratts, E.B. & Raut, A.G. (2004). Entropy Generation Minimization of Fully Developed Internal Flow with Constant Heat Flux. *Journal of Heat Transfer - ASME Transactions*, Vol. 126, pp. 656-659, ISSN 0022-1481.
- Renaud, L.; Malhaire, C. & Kleimann, P. (2008). Theoretical and Experimental Studies of Microflows in Silicon Microchannels. *Materials Science & Engineering C-Biomimetic and Supramolecular Systems*, Vol. 28, pp. 910-917, ISSN 0928-4931.
- Richardson, D.H.; Sekulic, D.P. & Campo, A. (2000). Low Reynolds Number Flow Inside Straight Micro Channels with Irregular Cross Sections. *Heat and Mass Transfer*, Vol. 36, pp. 187-193, ISSN 0947-7411.
- Sahin, A.Z. (1998). Second-Law Analysis of Laminar Viscous Flow through a Duct Subjected to Constant Wall Temperature. *Journal of Heat Transfer - ASME Transactions*, Vol. 120, pp. 77-83, ISSN 0022-1481.
- Sahin, A.Z.; Zubair, S.M.; Al-Garni, A.Z. & Kahraman, R. (2000). Effect of Fouling on Operational Cost in Pipe Flow due to Entropy Generation. *Energy Conversion and Management*, Vol. 41, pp. 1485-1496, ISSN 0196-8904.
- Stewart, S.W.; Shelton, S.V. & Aspelund, K.A. (2005) Finned-Tube Heat Exchanger Optimization Methodology. *Heat Transfer Engineering*, Vol. 26, pp. 22-28, ISSN 0145-7632
- Vicente, P.G.; Garcia, A. & Viedma, A. (2002). Experimental Study of Mixed Convection and Pressure Drop in Helically Dimpled Tubes for Laminar and Transition Flow. *International Journal of Heat and Mass Transfer*, Vol. 45, pp. 5091-5105, ISSN 0017-9310.
- Vijayalakshmi, K.; Anoop, K.B. & Patel, H.E. (2009). Effects of Compressibility and Transition to Turbulence on Flow through Microchannels. *International Journal of Heat and Mass Transfer*, Vol. 52, pp. 2196-2204, ISSN 0017-9310.
- Wang, H.; Wang, Y. & Zhang, J. (2005). Influence of Ribbon Structure Rough Wall on the Microscale Poiseuille Flow. *Journal of Fluids Engineering - ASME Transactions*, Vol. 127, pp. 1140-1145, ISSN 0098-2202.

- Wen, M.Y.; Jang, K.J. & Yang, C.C. (2003). Augmented Heat Transfer and Pressure Drop of Strip-Type Inserts in the Small Tubes. *Heat and Mass Transfer*, Vol. 40, pp. 133-141, ISSN 0947-7411.
- White, F.M. (1999). *Fluid Mechanics*, McGraw-Hill, ISBN 0-07-116848-6, Singapore.
- Wu, H.Y. & Cheng, P. (2003). An Experimental Study of Convective Heat Transfer in Silicon Microchannels with Different Surface Conditions. *International Journal of Heat and Mass Transfer*, Vol. 46, pp. 2547-2556, ISSN 0017-9310.
- Wu, J.S. & Tseng, K.C. (2001). Analysis of Micro-Scale Gas Flows with Pressure Boundaries using Direct Simulation Monte Carlo Method. *Computers and Fluids*, Vol. 30, pp. 711-735, ISSN 0045-7930.
- Wu, P. & Little, W.A. (1983). Measurement of Friction Factors for the Flow of Gases in very Fine Channels used for Microminiature Joule-Thompson Refrigerators. *Cryogenics*, Vol. 23, pp. 273-277, ISSN 0011-2275.
- Yilbas, B.S. & Pakdemirli, M. (2005) Entropy Generation Due to the Flow of a Non-Newtonian Fluid with Variable Viscosity in a Circular Pipe. *Heat Transfer Engineering*, Vol. 26, pp. 80-86, ISSN 0145-7632
- Yu, D.; Warrington, R.; Baron, R. & Ameel, T. (1995). An Experimental and Theoretical Investigation of Fluid Flow and Heat Transfer in Microtubes, *ASME/JSME Thermal Engineering Conference*, pp. 523-530.
- Zimparov, V. (2000). Extended Performance Evaluation Criteria for Enhanced Heat Transfer Surfaces: Heat Transfer through Ducts with Constant Wall Temperature. *International Journal of Heat and Mass Transfer*, Vol. 43, pp. 3137-3155, ISSN 0017-9310.





## **Evaporation, Condensation and Heat transfer**

Edited by Dr. Amimul Ahsan

ISBN 978-953-307-583-9

Hard cover, 582 pages

**Publisher** InTech

**Published online** 12, September, 2011

**Published in print edition** September, 2011

The theoretical analysis and modeling of heat and mass transfer rates produced in evaporation and condensation processes are significant issues in a design of wide range of industrial processes and devices. This book includes 25 advanced and revised contributions, and it covers mainly (1) evaporation and boiling, (2) condensation and cooling, (3) heat transfer and exchanger, and (4) fluid and flow. The readers of this book will appreciate the current issues of modeling on evaporation, water vapor condensation, heat transfer and exchanger, and on fluid flow in different aspects. The approaches would be applicable in various industrial purposes as well. The advanced idea and information described here will be fruitful for the readers to find a sustainable solution in an industrialized society.

### **How to reference**

In order to correctly reference this scholarly work, feel free to copy and paste the following:

A. Alper Ozalp (2011). Fluid Mechanics, Heat Transfer and Thermodynamic Issues of Micropipe Flows, Evaporation, Condensation and Heat transfer, Dr. Amimul Ahsan (Ed.), ISBN: 978-953-307-583-9, InTech, Available from: <http://www.intechopen.com/books/evaporation-condensation-and-heat-transfer/fluid-mechanics-heat-transfer-and-thermodynamic-issues-of-micropipe-flows>

**INTECH**  
open science | open minds

### **InTech Europe**

University Campus STeP Ri  
Slavka Krautzeka 83/A  
51000 Rijeka, Croatia  
Phone: +385 (51) 770 447  
Fax: +385 (51) 686 166  
[www.intechopen.com](http://www.intechopen.com)

### **InTech China**

Unit 405, Office Block, Hotel Equatorial Shanghai  
No.65, Yan An Road (West), Shanghai, 200040, China  
中国上海市延安西路65号上海国际贵都大饭店办公楼405单元  
Phone: +86-21-62489820  
Fax: +86-21-62489821

© 2011 The Author(s). Licensee IntechOpen. This chapter is distributed under the terms of the [Creative Commons Attribution-NonCommercial-ShareAlike-3.0 License](#), which permits use, distribution and reproduction for non-commercial purposes, provided the original is properly cited and derivative works building on this content are distributed under the same license.